ORIGINAL ARTICLE

lajss.org© Latin American Journal of Solids and Structures

www.lajss.org

Influence of the excitation frequency content on the efficiency of a tuned liquid column damper

G. Espinoza[a]*, C. Romero[a], F. Benedetti[a]

[a] Department of Civil and Environmental Engineering. University of Bío-Bío. Avenida Collao 1202. Concepción. Chile. E-mail: gespinoz@ubiobio.cl, cromeror@egresados.ubiobio.cl, fbenedet@ubiobio.cl

* Corresponding author

https://doi.org/10.1590/1679-78256321

Abstract

The current study addresses the influence of the excitation frequency content on the efficiency of a tuned liquid column damper (TLCD) to control the displacement response in structures subjected to seismic excitations. A time-domain stochastic stationary analysis is performed, and an equivalent statistical linearization for the TLCD is obtained. The results show that the TLCD is more efficient in structures subjected to broadband processes. In narrowband processes, the maximum performance of the TLCD occurs when the linear equivalent period of the system TLCD-structure tunes the TLCD period, and the frequency of the structure matches the predominant frequency of the input motion. Results derived from this analysis are validated through two time-history seismic analyses.

Keywords

Passive control; tuned liquid column dampers; frequency content; stochastic analysis; equivalent statistical linearization

Graphical Abstract

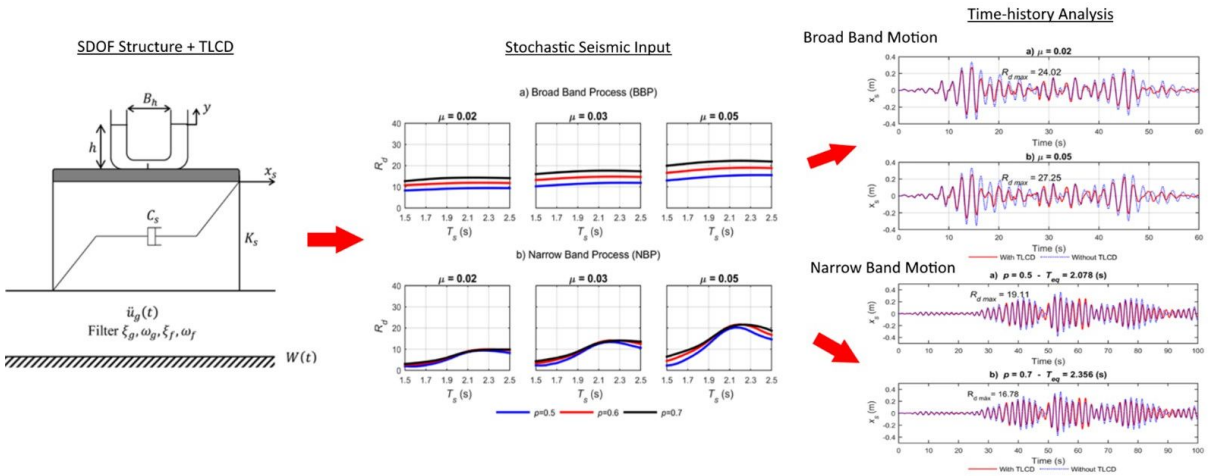

Received November 03, 2020. In revised form June 07, 2021. Accepted September 20, 2021. Available online September 20, 2021.
https://doi.org/10.1590/1679-78256321

1 INTRODUCTION

Different devices have emerged as alternatives to the seismic design, satisfying design requirements when added to the structure and then modifying its dynamic properties. Diverse researchers have studied the efficiency of tuned damper systems to control the inertial effect (e.g. Den Hartog, 1956; Sadek et al., 1997; Lin et al., 2000; Ueng et al., 2008; Almazán et al., 2012). For instance, some of them have proposed tuned mass damper (TMD) and the tuned liquid column damper (TLCD). Tuned liquid dampers (TLD) have turned into one of the most usual devices to control structural vibrations since they are cost-effective and easy to install. These devices are classified into TLCD and tuned sloshing damper (TSD). The TLCD consists of a U-shaped container, filled generally with water. The oscillation of the liquid column has a frequency that depends on the properties of the TLCD, and the U-shaped container has a hole in its lower horizontal part that produces a head loss.

First investigations have been focused on determining optimum properties of the TLCD for the control of structures subject to wind loads. Xu et al. (1992) studied the behavior of the TLCD as a solution to mitigate vibrations due to wind excitations. They compared the TLCD performance with the TMD efficacy, concluding that the TLCD presents practical advantages and counts on an efficiency similar to the TMD.

Optimum parameter estimations for TLCD design purposes have also been proposed. For instance, Wu et al. (2005) performed an experimental analysis of free and harmonic structure response through a shaking table, providing empirical equations to assist the design of the TLCD. They concluded that the liquid mass and the length ratio (geometrical property of the TLCD corresponding to the ratio between the horizontal separation of the liquid columns and the total water length contained in the tube) of the TLCD do not affect the natural frequency and the optimum head loss of the TLCD. In Shum (2009), a closed-form solution for TLCD optimum parameter calculation is proposed to attenuate the building's maximum displacement response.

Xu & Shum (2003) studied multiple units of TLCD (MTLCDs) to reduce torsional vibrations in asymmetric structures to estimate their optimum parameters. These researchers concluded that the MTLCD is more efficient than a single TLCD (STLCD). However, when the number of MTLCDs is higher than five, MTLCD efficiency diminishes. Lee et al. (2010) experimentally investigated the dynamic response of a TLCD specimen subjected to harmonic loading with various excitation amplitudes using a shaking table. They concluded that the natural frequency and the mass ratio (quotient between the liquid mass and the mains structure mass) are independent of the amplitude excitation variation, while the damping ratio of a TLCD increases with larger amplitudes.

Chakraborty et al. (2011) analyzed the behavior of the TLCD when the structure displacement response is minimized, considering the influence of the maximum displacement of the liquid column within TLCD and estimating optimum parameters. Rozas et al. (2015) studied a device composed of two independent and orthogonally TLCDs for controlling the seismic response of structures. According to the authors, this TLCD arrangement requires less liquid than two equivalent and independent TLCDs. Their results show that this arrangement has higher displacement reductions for low damping ratios and decreases its efficiency as the structure-damping ratio increases.

Altunişik et al. (2017) also performed an experimental study of a prototype consisting of four columns joined to a top and bottom plate. The prototype is excited through a shaking table in different directions. The authors reported optimum parameters that were obtained experimentally and numerically. They concluded that the TLCD causes to decrease the resonance frequency and a damping ratio increment.

Park et al. (2018) proposed a different passive damper and TLCD based. The proposed damping mechanism is a conventional TLCD using embossments in its inner walls. The researchers named this device ETLCD (TLCD with embossments). The study focused on an experimental evaluation of the ELTCD dynamic characteristics and its vibration control performance for tall buildings. The results suggest that ETLCD is more efficient than the TLCD in terms of amplitude response reduction.

Concerning the effect of the seismic demand properties on the response of the TLCD, a number of studies can be highlighted. Kavand & Zahrai (2006a, 2006b), and Zahrai & Kavand (2008) studied the impact of the characteristics of the frequency content and soil conditions on the efficiency of a TLCD by means of nonlinear time-history analyses using actual seismic records. They showed a notorious effect of these properties on the effectiveness of the TLCD, finding that the efficiency in the reduction of the acceleration response is not significant.

Based on the known researches carried out so far, it is observed that the influence of the seismic excitation frequency content in TLCD performance needs to be addressed. Although there are important efforts in this subject, a wider understanding is needed in order to assess its effect in the TLCD's optimal design parameters and effectiveness to reduce the displacements and accelerations.

Consequently, the current research aims to analyze the behavior of the optimum parameters and the TLCD efficiency when the structure is subject to excitations with different frequency content. To have precise and accurate

control of the freuquncy content of the seismic demands, and also to optimize the computation effort, the analysis is performed using and stochastic stationary approach.

2 MODEL AND EQUATION OF MOTION

2.1 Model with TLCD

The model considered for this study is presented in Figure 1. The model comprises a single-degree-of-freedom linear system with a TLCD attached. This device is a U-shaped container and has an orifice plate inside its horizontal section.

The variables considered to obtain the equations of motion corresponds to the elastic stiffness (K_s); damping (C_s) and mass (m_s) of the main system, respectively. The symbol B_h defines the length of the horizontal section of the container, and h is the liquid column's height. The variable x_s denotes the main structure's displacement, while y corresponds to the liquid surface displacement in the column. The ground acceleration has been denoted as $\ddot{u}_g$.

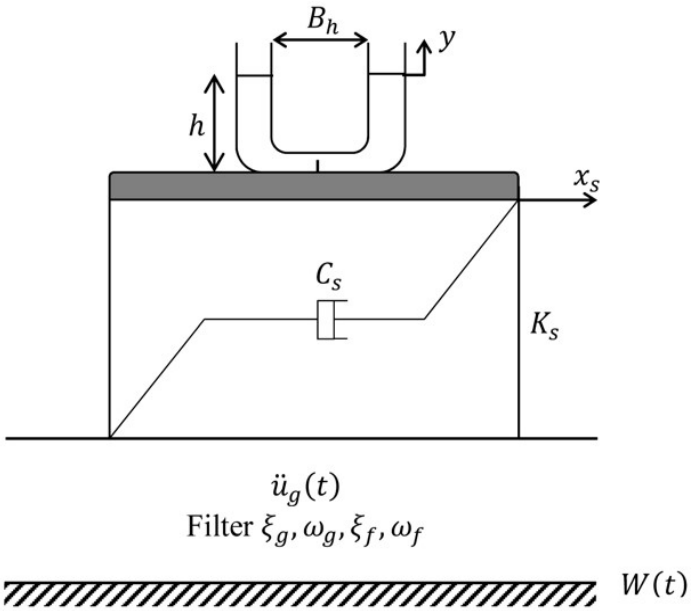

Figure 1 Linear structure model with TLCD attached.

2.2 Equations of motion of the TLCD – main structure system

The studied system is a two-degree-of-freedom model: the vertical displacement of the liquid in the tube and the lateral displacement of the main structure. The model is excited at the base by an acceleration $\ddot{u}_g$.

The motion equations are expressed in Eq.1 (Sakai et al., 1989) and Eq.2 (Chakraborty et al., 2012).

$$\rho A L_e \ddot{y} + \frac{1}{2}\rho \xi A |\dot{y}| \dot{y} + 2\rho g A y = -\rho A B_h \left(\ddot{x} + \ddot{u}_g\right) \tag{1}$$

$$(m_s + \rho A B_h + 2\rho h A)\ddot{x} + C_s \dot{x} + K_s x = -(m_s + \rho A B_h + 2\rho h A)\ddot{u}_g - \rho A B_h \ddot{y} \tag{2}$$

Where $L_e = 2h + B_h$ is the total liquid column length, ρ is the density of the liquid, A is the area of the cross-section, and g is the gravity acceleration. The head loss coefficient corresponds to ξ, and it depends on the orifice diameter in the plate inside the U-tube horizontal section.

From the model motion equations, it is observed that Eq.1 is nonlinear; therefore, it must be linearized through the equivalent statistical linearization method (Iwan & Yang, 1972). This method consists of the replacement of the nonlinear term in the motion equations by a linear coefficient, corresponding to C_p, that relies on an element of the covariance matrix, which in turn also depends on the C_p value, implying that the process is iterative.

Linearizing statistically Eq.1 yields:

$$\rho A L_e \ddot{y} + 2\rho A C_p \dot{y} + 2\rho g A y = -\rho A B_h \left(\ddot{x} + \ddot{u}_g\right) \tag{3}$$

where the C_p value, for a zero-mean Gaussian stationary process, can be calculated as:

$$C_p = \frac{\xi \sigma_{\dot{y}}}{\sqrt{2\pi}} \tag{4}$$

Eq. 4 shows the equivalent damping coefficient C_p, being $\sigma_{\dot{y}}$ the standard deviation of the liquid velocity. By normalizing Eq. 3 with respect to the liquid mass $\rho A L_e$, Eq.5 is obtained:

$$\ddot{y} + \frac{2C_p}{L_e}\dot{y} + \frac{2g}{L_e}y + p\ddot{x} = -p\ddot{u}_g \tag{5}$$

Where $p = B_h/L_e$ is the length ratio of the TLCD.

From Eq. 5, the natural frequency of the liquid column is $\omega_l = \sqrt{2g/L_e}$, where $\gamma = \omega_l/\omega_s$ is the tuning ratio with respect to the natural frequency of the main structure ω_s.

On the other hand, Eq.2 can be rewritten as

$$(m_s + m_l)\ddot{x} + C_s\dot{x} + K_s x = -(m_s + m_l)\ddot{u}_g - \rho A p L_e \ddot{y} \tag{6}$$

where $m_l = \rho A B_h + 2\rho h A$ is the mass of the liquid.

The term μ stands for the ratio between the mass of the liquid and the main structure mass, i.e., $\mu = \rho A L_e/m_s$. Normalizing Eq. 6 with respect to the mass m_s

$$(1+\mu)\ddot{x} + \frac{C_s}{m_s}\dot{x} + \frac{K_s}{m_s}x = -(1+\mu)\ddot{u}_g - \mu p\ddot{y} \tag{7}$$

The parameters $\omega_s = \sqrt{K_s/m_s}$ and $\xi_s = C_s/(2m_s\omega_s)$ are the natural frequency and damping of the main structure. Therefore, Eq. 7 becomes into Eq. 8 as follows:

$$(1+\mu)\ddot{x} + 2\xi_s\omega_s\dot{x} + \omega_s^2 x + \mu p\ddot{y} = -(1+\mu)\ddot{u}_g \tag{8}$$

Expressing Eq. 5 and 8 in matrix form results

$$\mathbf{M}\ddot{\mathbf{X}} + \mathbf{C}\dot{\mathbf{X}} + \mathbf{K}\mathbf{X} = -\mathbf{R_1}\ddot{u}_g \tag{9}$$

$$\mathbf{X} = \{y \quad x\}^T \tag{10}$$

Where

$$\mathbf{M} = \begin{bmatrix} 1 & p \\ \mu p & (1+\mu) \end{bmatrix} \quad \mathbf{C} = \begin{bmatrix} \frac{2C_p}{L_e} & 0 \\ 0 & 2\xi_s\omega_s \end{bmatrix} \quad \mathbf{K} = \begin{bmatrix} \frac{2g}{L_e} & 0 \\ 0 & \omega_s^2 \end{bmatrix} \quad \mathbf{R_1} = \begin{Bmatrix} p \\ (1+\mu) \end{Bmatrix} \tag{11}$$

Hence

$$\begin{bmatrix} 1 & p \\ \mu p & (1+\mu) \end{bmatrix} \begin{Bmatrix} \ddot{y} \\ \ddot{x} \end{Bmatrix} + \begin{bmatrix} \frac{2C_p}{L_e} & 0 \\ 0 & 2\xi_s\omega_s \end{bmatrix} \begin{Bmatrix} \dot{y} \\ \dot{x} \end{Bmatrix} + \begin{bmatrix} \frac{2g}{L_e} & 0 \\ 0 & \omega_s^2 \end{bmatrix} \begin{Bmatrix} y \\ x \end{Bmatrix} = -\begin{Bmatrix} p \\ (1+\mu) \end{Bmatrix} \ddot{u}_g \tag{12}$$

The vector $\mathbf{X}$ denotes the TLCD-main structure system degrees of freedom vector, while M denotes the mass matrix, $\mathbf{C}$ and $\mathbf{K}$ are the damping and stiffness matrices of the system. The matrix $\mathbf{R_1}$ is the influence matrix of the input, defined in Eq.11.

3 SEISMIC EXCITATION

A time-domain stochastic analysis was performed on the model, considering the two random processes: broad bandwidth (BBP) and narrow bandwidth (NBP). A Clough-Penzien double filter was used to characterize the frequency content of the seismic excitation. The Clough-Penzien double filter consisted of a filter derived from the soil layer's properties and an additional filter for the low frequencies. The parameters that characterize the Ckough-Penzien double filter for the random process of broad bandwidth (high content of frequencies) and narrow bandwidth (low-frequency content) are given in Table 1.

The BBP filter parameters were estimated employing the least-squares adjustment of the Power Spectral Density (PSD) function. The PSD was calculated for an artificial earthquake compatible with the NCh2745:2013 (INN, 2013) B soil class elastic spectrum. According to this standard, a B soil type represents a soil profile with a shear wave velocity V_{s30} larger than 500 m/s (but lower than 900 m/s). The NBP filter was obtained through the parameter setting to establish a narrow bandwidth motion compatible with the component N90E of the SCT station of the 1985 Mexico earthquake recording. The predominant period of the narrow bandwidth filter was $T_p = 1.93$ seconds generated by a very soft layer of clay with shear wave velocities between 60 m/s to 100 m/s (Mayoral et al., 2019).

The seismic motions defined as objective inputs for the stochastic stationary processes are presented in Figure 2. For both BBP and NBP cases, this figure shows the acceleration time series considered to define the mean Power Spectral Density (mean PSD) from which the modified Clough-Penzien double filter (Modified CPF) is derived and adjusted. In the case of the BBP process, the power spectral density denotes a broad frequency content, with frequencies ranging from 0.2 Hz to around 6 Hz. Moreover, for the NBP case the narrow frequency content is concentrated at approximately 0.5 Hz. Additionally, the response spectrum is shown to better characterize the seismic demands, evidencing the NBP artificial earthquake motion fitting to the elastic spectrum of the B soil class NCh2745:2013 code (INN, 2013).

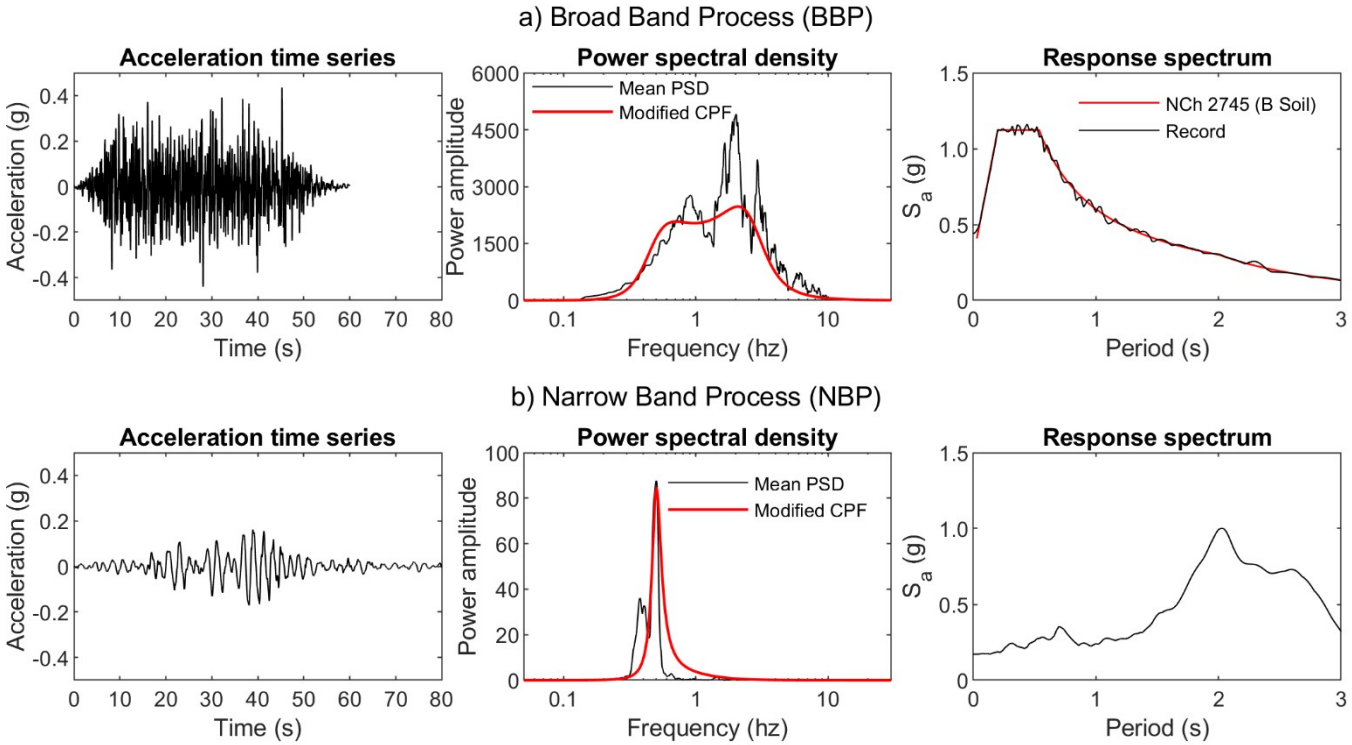

Figure 2 Stochastic seismic demands characterization for BBP and NBP processes.

Table 1 Clough-Penzien filter parameters for the two random processes considered.

	Parameters				
Process	S_0	$\omega_g\ (rad/s)$	ξ_g	$\omega_f\ (rad/s)$	ξ_f
BBP	1335.6	16.57	0.491	3.02	0.48
NBP	207.23	3.14	0.1	8.48	0.9

The modified Clough-Penzien filter equation is defined as follows (Clough & Penzien, 1975).

$$S_g(\omega) = S_0 \frac{\omega_g^4 + 2\xi_g^2\omega_g^2\omega^2}{\left(\omega_g^2-\omega^2\right)^2 + 4\xi_g^2\omega_g^2\omega^2} \cdot \frac{\omega^4}{\left(\omega_f^2-\omega^2\right)^2 + 4\xi_f^2\omega_f^2\omega^2} \tag{13}$$

Where $S_0, \omega_g, \omega_f, \xi_f, \xi_g$ are the filter parameters to be adjusted. The variable S_0 is the white noise intensity; ω_g and ω_f stand for the soil layer frequency and the filter frequency, respectively. The variables ξ_g and ξ_f denote the damping coefficients of the soil and the filter, respectively.

4 PROBABILISTIC ANALYSIS IN TIME DOMAIN

4.1 State-space representation

The state-space representation of the main structure with TLCD, and the state vector, are shown in Eq.14, Eq.15, and Eq.16, respectively. The $\mathbf{A}$ and $\mathbf{B_u}$ matrices (Eq.17 and Eq.18) are the state and influence matrices of the input. The $\mathbf{X_1}$ vector is the state vector (Eq.16). The soil acceleration is defined by the output equation (Eq.15), which depends on the response vector of the filter, $\mathbf{X_f}$ (Eq.19), and the filter matrix, $\mathbf{C_f}$ (Eq. 21), where the frequency content of the input is stated. Eq. 18 represents the filter state equation. The state matrices of the filter, $\mathbf{A_f}$ and $\mathbf{B_f}$, are defined according to Eq.20 (Saitua et al., 2018).

$$\dot{\mathbf{X}}_\mathbf{1} = \mathbf{A}\mathbf{X_1} + \mathbf{B_u}\ddot{u}_g \tag{14}$$

$$\ddot{u}_g = \mathbf{C_f}\mathbf{X_f} \tag{15}$$

$$\mathbf{X_1} = \{y \quad x \quad \dot{y} \quad \dot{x}\}^T \tag{16}$$

$$\mathbf{A} = \begin{bmatrix} \mathbf{0}_{2x2} & \mathbf{I}_{2x2} \\ -\mathbf{M}^{-1}\mathbf{K} & -\mathbf{M}^{-1}\mathbf{C} \end{bmatrix} \tag{17}$$

$$\mathbf{B} = \begin{bmatrix} \mathbf{0}_{2x2} \\ -\mathbf{M}^{-1}\mathbf{R} \end{bmatrix} \tag{18}$$

$$\dot{\mathbf{X}}_\mathbf{f} = \mathbf{A_f}\mathbf{X_f} + \mathbf{B_f}W(t) \tag{19}$$

$$\mathbf{X_f} = \{x_g \quad \dot{x}_g \quad x_f \quad \dot{x}_f\}^T \tag{20}$$

$$\mathbf{A_f} = \begin{bmatrix} 0 & 1 & 0 & 0 \\ -\omega_g^2 & -2\xi_g\omega_g & 0 & 0 \\ 0 & 0 & 0 & 1 \\ \omega_g^2 & 2\xi_g\omega_g & -\omega_f^2 & -2\xi_f\omega_f \end{bmatrix} \quad \mathbf{B_f} = \begin{Bmatrix} 0 \\ -1 \\ 0 \\ 0 \end{Bmatrix} \tag{21}$$

$$\mathbf{C_f} = \begin{bmatrix} \omega_g^2 & 2\xi_g\omega_g & -\omega_f^2 & -2\xi_f\omega_f \end{bmatrix} \tag{22}$$

The Eq.24 is the extended state equation, that is, the main structure-TLCD-filter. Therefore, the variable $\mathbf{X_2}$ is the extended state vector, and it contains the state vector of the main structure-TLCD system and the status vector of the filter (Eq.23). The matrices of the expanded system state equation are the state matrix $\mathbf{A_2}$ and the input matrix $\mathbf{B_2}$, and they are shown in Eq.25.

$$\mathbf{X_2} = \{\mathbf{X_1} \quad \mathbf{X_f}\}^T \tag{23}$$

$$\dot{\mathbf{X}}_\mathbf{2} = \mathbf{A_2}\mathbf{X_2} + \mathbf{B_2}W(t) \tag{24}$$

$$\mathbf{A_2} = \begin{bmatrix} \mathbf{A} & \mathbf{B}\mathbf{C_f} \\ \mathbf{0} & \mathbf{A_f} \end{bmatrix} \quad \mathbf{B_2} = \begin{Bmatrix} \mathbf{0} \\ \mathbf{B_f} \end{Bmatrix} \tag{25}$$

4.2 Covariance matrix calculation

The covariance matrix was calculated from the Lyapunov equation (Eq. 27) solution, assuming a steady-state and white noise as input. As depicted in Eq. 26, the soil acceleration variance was considered to calculate the white noise intensity as a function of time.

$$\sigma_{\ddot{u}_g}^2 = \frac{PGA}{3} \tag{26}$$

Where the PGA (Peak Ground Acceleration) taken into account was 0.25g to ensure the linearity of the main system.

$$\mathbf{A_2^T R + R A_2 + B_2^T} W(t) \mathbf{B_2} = \mathbf{0} \tag{27}$$

In Eq. (27) $\mathbf{R}$ defines the covariance matrix of the complete main structure-TCLD-filter system.

4.3 Optimization procedure

The TLCD design parameters addressed were the frequency ratio γ and its head loss coefficient ξ. They were optimized by establishing an objective function to minimize the standard deviation of the main structure displacement (Eq.28), subject to the height restriction of the liquid inside the U-tube container, as shown in Eq.29c.

$$Mininize: J(\gamma, \xi) = Min(\sigma_x) \tag{28}$$

$$0.5 < \gamma < 1.5 \tag{29a}$$

$$0.01 < \xi < 30 \tag{29b}$$

$$h - c\sigma_y \geq 0 \tag{29c}$$

Where c is a safety factor that avoids air ingress to the horizontal line where the energy is dissipated.

5 RESULTS AND DISCUSSION

5.1 Analysis of the system characteristics influence

The sensitivity of each TLCD optimum parameter was analyzed, with respect to the following system parameters: the mass ratio (Figures 3 and 4), the length ratio (Figures 5 and 6), the main structure damping (Figures 7 and 8), and the main structure period (Figures 9 and 10). The first row shows the optimum TLCD tuning ratio in all those figures, and the second row shows its optimum head loss coefficient.

5.1.1 Influence of the mass ratio $\boldsymbol{\mu}$

Figures 3 and 4 collect three length ratios of the TLCD $(p = 0.5, 0.6, 0.7)$ and three main structure periods sets $(T_s = 1.5, 2.0, 2.5\ s)$ to show the optimum TLCD parameters as functions of mass ratio (μ) for BBP and NBP cases.

The behavior of the TLCD design parameters depends strongly on the frequency content of the excitation. For the BBP, as it is depicted in the upper graphs of Figure 3, the optimum frequency ratio of the TLCD (γ_{opt}) does not depend on the value of the length ratio of the TLCD. In contrast, as shown in the upper graphs in Figure 4, for the NBP excitations, the optimum frequency ratio depends on the value of the length ratio of the TLCD. Furthermore, γ_{opt} is also sensitive to the structure flexibility, but is not dependent on the p value for high values of the main structure period.

Besides, the optimum head loss coefficient (ξ_{opt}) also shows a different behavior relying on the type of excitation. For BBP (lower graphs of Figure 3), it is showed a linear decrease up to a specific mass ratio value where a slope change occurs, which depends on the value of the length ratio of the TLCD. While the p value is higher, the mass ratio length ratio value, at a slope change occurs, will also be higher.

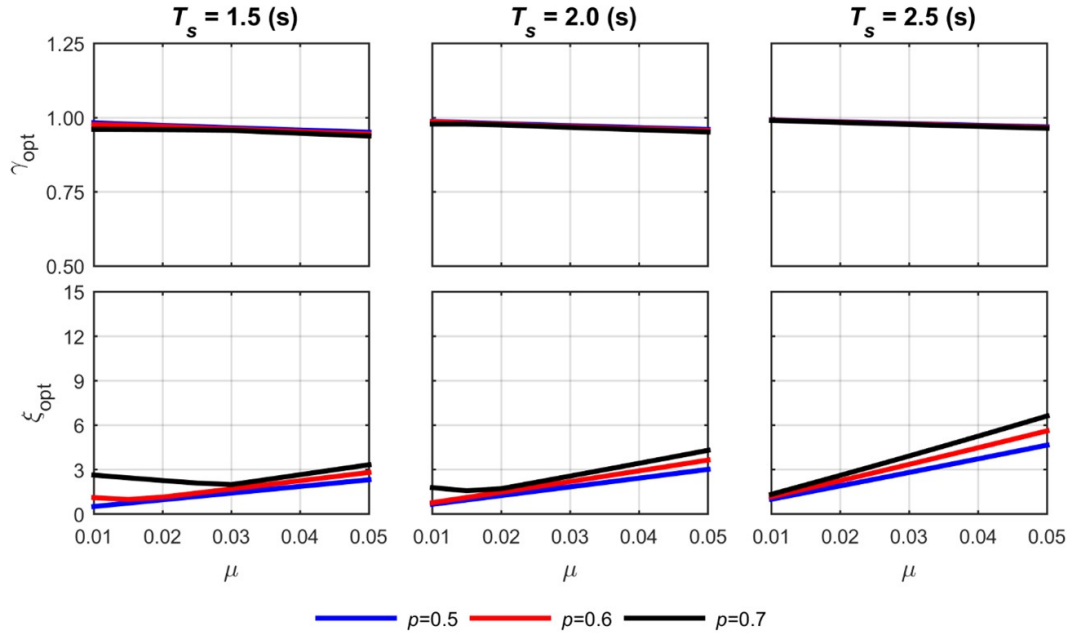

Figure 3 Optimum tuning ratio (γ_{opt}) and head loss coefficient (ξ_{opt}) as functions of the mass ratio (μ), with a system damping $\xi_s = 0.05$ for a BBP.

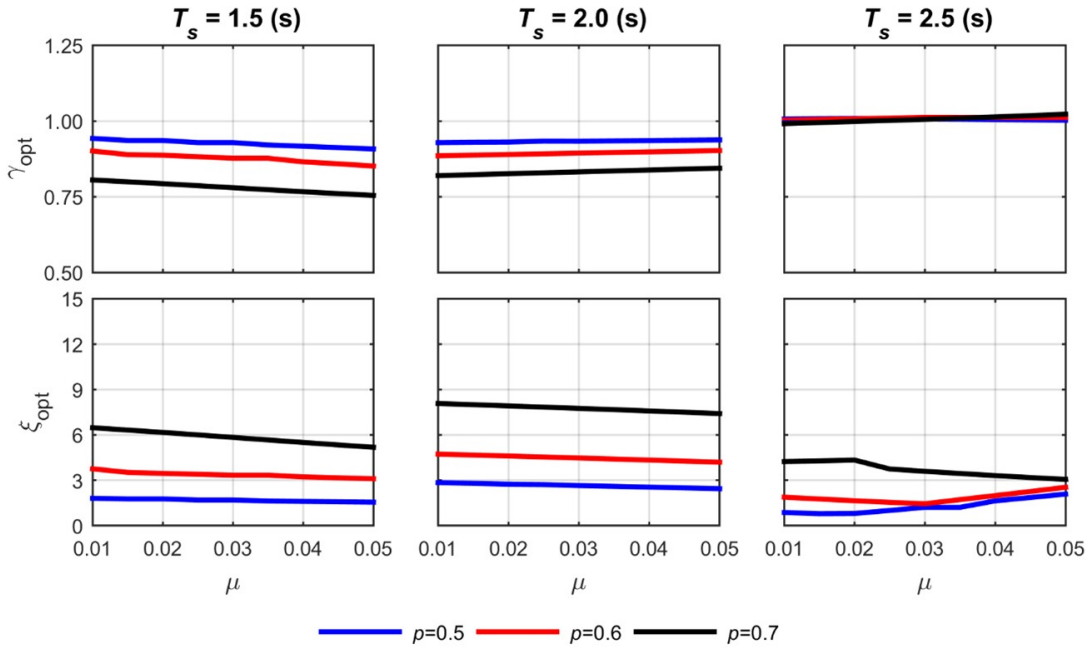

Figure 4 Optimum tuning ratio (γ_{opt}) and head loss coefficient (ξ_{opt}) as functions of the mass ratio (μ), with a system damping $\xi_s = 0.05$ for a NBP.

5.1.2 Influence of the length ratio of the TLCD $\boldsymbol{p}$

Figures 5 and 6 represents three mass ratios of the TLCD $(\mu = 0.02, 0.03, 0.05)$ and three main structure periods sets $(T_s = 1.5, 2.0, 2.5\ s)$, to address the influence of the length ratio of the TLCD on the optimum TLCD parameters for the BBP and NBP cases, respectively.

Similarly to Figure 3, the TLCD design parameters behavior depends on the frequency content of the excitation. While in BBP, the TLCD is perfectly tuned to the main structure and is insensitive to the mass ratio and the flexibility of the structure (see upper graphs in Figure 5). For the NBP case, the optimum tuning ratio depends on the main structure period (see upper graphs in Figure 6). On the other hand, the value of the optimum TLCD head loss coefficient (ξ_{opt}) varies differently with respect to the length ratio of TLCD and the main structure period for BBP or NBP cases (see lower graphs in figures 5 and 6, respectively).

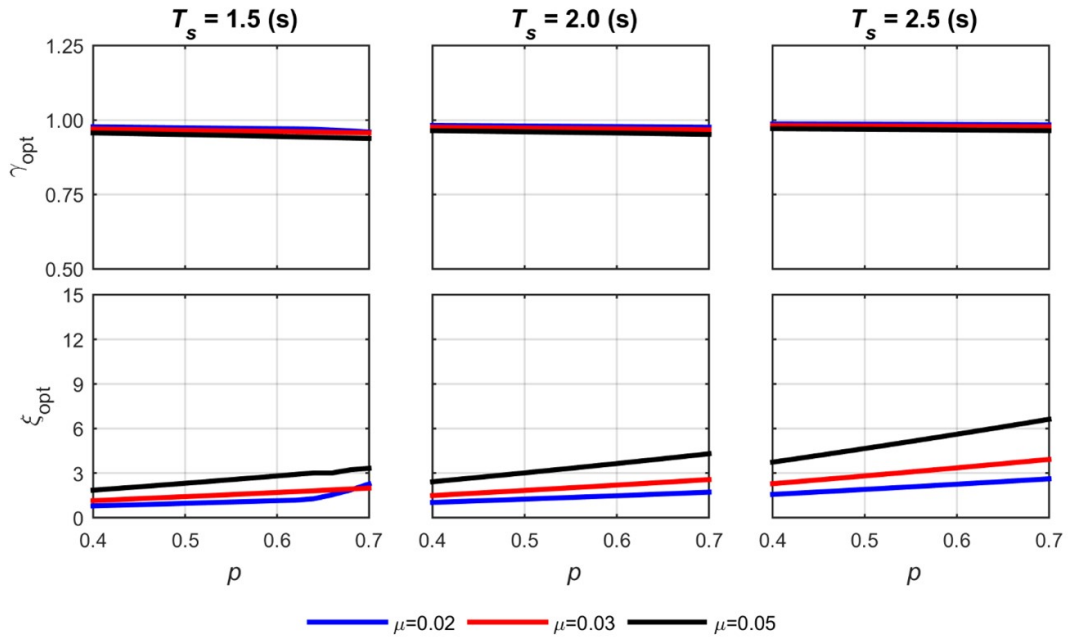

Figure 5 Optimum tuning ratio (γ_{opt}) and head loss coefficient (ξ_{opt}) as functions of the length ratio (p), with a system damping $\xi_s = 0.05$ for a BBP.

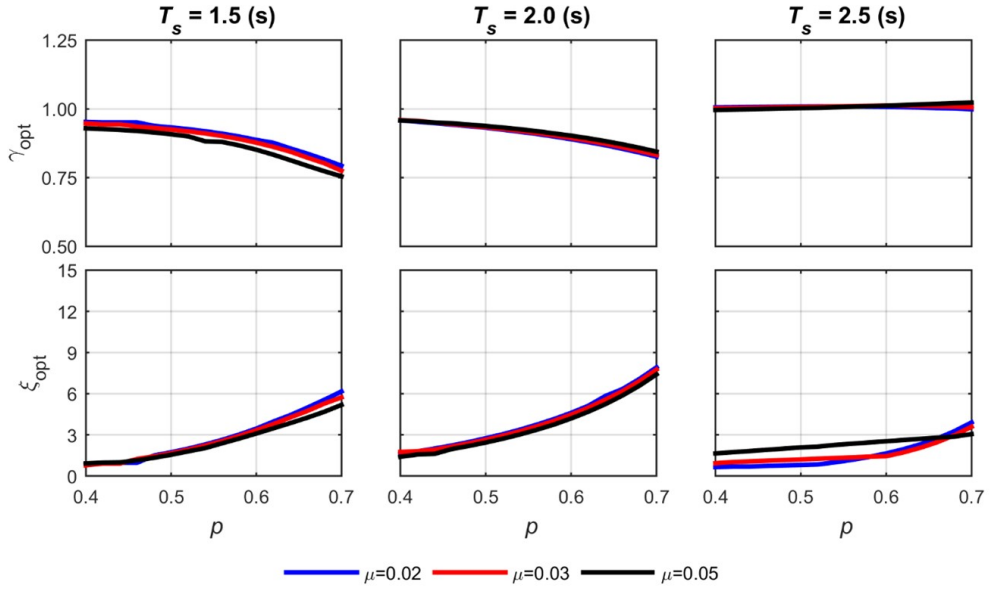

Figure 6 Optimum tuning ratio (γ_{opt}) and head loss coefficient (ξ_{opt}) as functions of the length ratio (p), with a system damping $\xi_s = 0.05$ for a NBP.

5.1.3 Influence of the main structure damping ξ

Figures 7 and 8 describe the behavior of the optimum TLCD parameters. For BBP and NBP cases, the same main structure and length ratio values are taken into account. Specifically, three periods are considered to analyze the influence of the main structure flexibility $(T_s = 1.5, 2.0, 2.5\ s)$, as well as three length ratios of the TLCD $(p = 0.5, 0.6, 0.7)$.

As in the case of μ and p parameters, there is a significant influence of the excitation frequency content on the optimum TLCD parameters. For BBP excitations, the tuning ratio of the TLCD is perfectly tuned to the main structure (see the upper graph in Figure 7). In addition, no influence on the tuning ratio of the TLCD (γ_{opt}) is noticed, due to neither structure flexibility nor to its length ratio variations. Conversely, for the NBP excitation case (see the upper figure in Figure 8), the tuning ratio of the TLCD varies as the length ratio and the period of the structure do, taking higher values for the shorter length ratios when period values are less than 2.0 s.

The frequency content also affects the behavior of the optimum head loss coefficient (ξ_{opt}). This influence is clearly noticed in the NBP case (lower graphs in Figure 8), where the optimum load loss coefficient value is increased when the structure period is $T_s = 2.0\ s$. This effect can be associated with a coincidence with the predominant period for the input, $T_p = 1.98\ s$. On the other hand, for the BBP demand, no significant effect of the main structure damping ratio occur, but for higher length ratios, ξ_{opt} is higher.

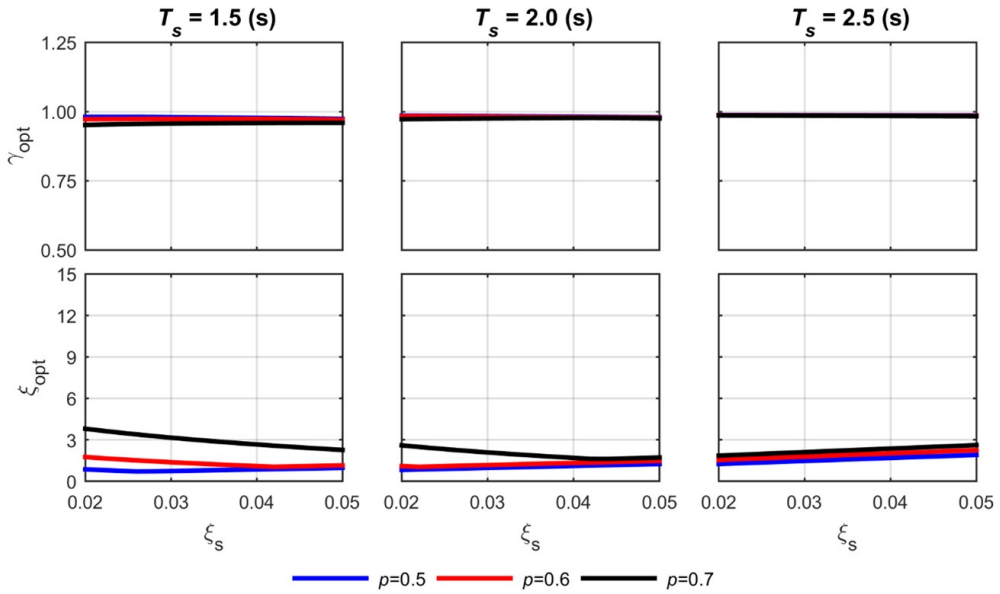

Figure 7 Optimum tuning ratio (γ_{opt}) and head loss coefficient (ξ_{opt}) as functions of the main system damping (ξ_s), with a mass ratio $\mu = 0.02$, for a BBP.

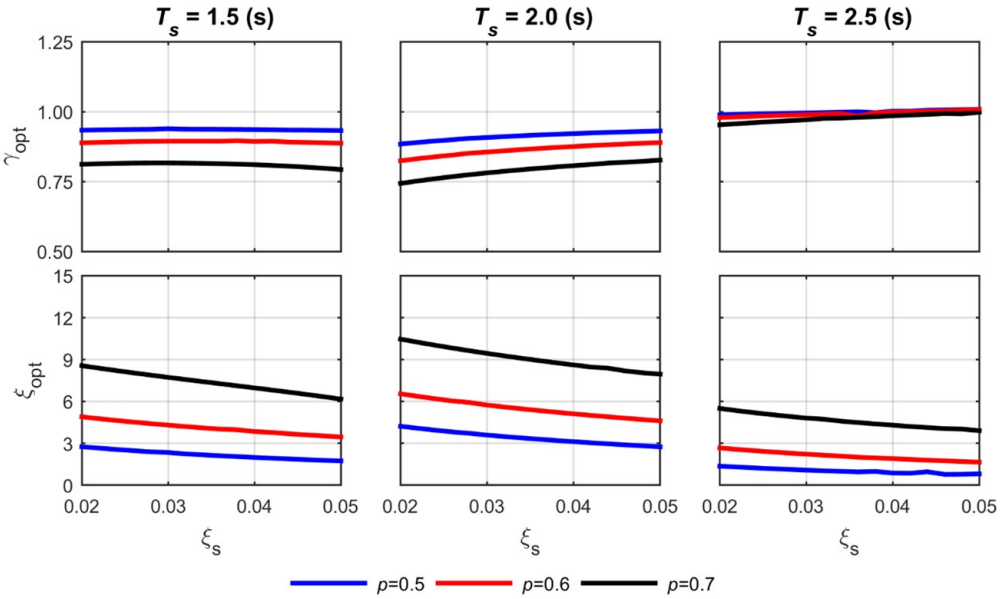

Figure 8 Optimum tuning ratio (γ_{opt}) and head loss coefficient (ξ_{opt}) as functions of the main system damping (ξ_s), with a mass ratio $\mu = 0.02$, for a NBP.

5.1.4 Influence of the main structure period T_s

Figures 9 and 10 are presented the optimum TLCD parameters as a function of the main structure period. Three mass ratios $(\mu = 0.02, 0.03, 0.05)$ and three length ratios of the TLCD $(p = 0.5, 0.6, 0.7)$ are considered for BBP and NBP cases.

The behavior of the optimum TLCD depends strongly on the frequency content of the excitation. In the BBP case, the optimum tuning ratio (γ_{opt}) tunes to the main structure period and does not depend on the length ratio. In the NBP case, the optimum tuning ratio shows a behavior that, practically, does not depend on the value of the mass ratio,

reaching a minimum at the period value that corresponds to the equivalent linear period of the main system with the TLCD (T_{eq}). This period value must also coincide with the predominant period of seismic excitation (T_p, Table 2).

Table 2 Optimum TLCD parameters for $T_{eq} = T_p = 1.982(s)$ NBP.

p	0.5			0.6			0.7		
μ	0.02	0.03	0.05	0.02	0.03	0.05	0.02	0.03	0.05
$\gamma_{opt} = \omega_{opt}/\omega_s$	0.8633	0.8585	0.8544	0.8229	0.8183	0.8109	0.7598	0.7565	0.7494
ξ_{opt}	2.1343	2.0435	1.8358	3.4025	3.2643	3.0058	5.8327	5.6929	5.2392
T_s	1.7157	1.7040	1.6549	1.6590	1.6510	1.5900	1.5540	1.5200	1.4900

The head loss coefficient does not depend on the mass ratio, but it is sensitive to the length ratio of the TLCD. However, the general behavior concerning the period depends on the frequency content of the excitation. While the head loss coefficient increases as the structure is more flexible for the BBP case, in the NBP case it reaches a maximum value when the period of the system matches the inflection point of the frequency ratio curves.

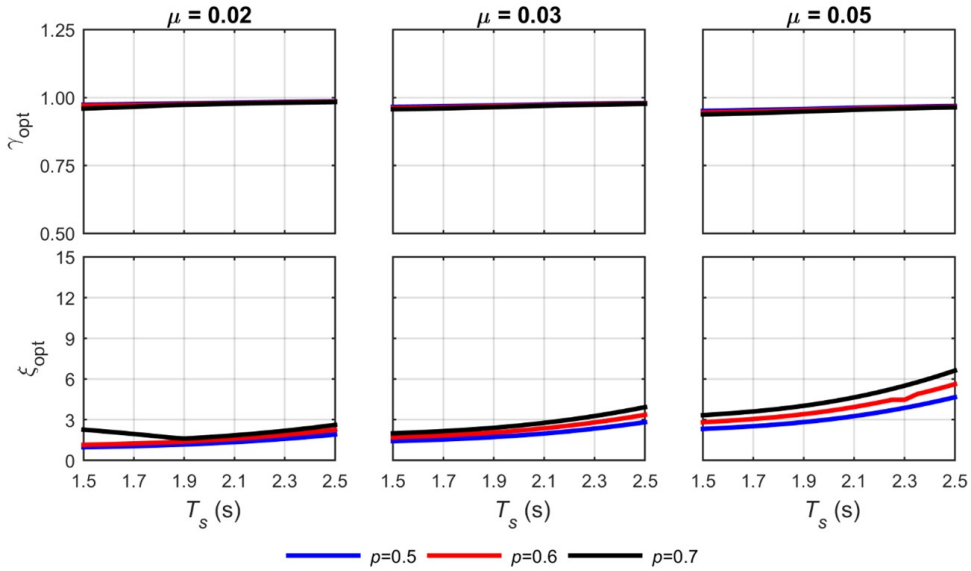

Figure 9 Optimum tuning ratio (γ_{opt}) and head loss coefficient (ξ_{opt}) as functions of the period of the primary structure (T_s), with a system damping $\xi_s = 0.05$, for a BBP.

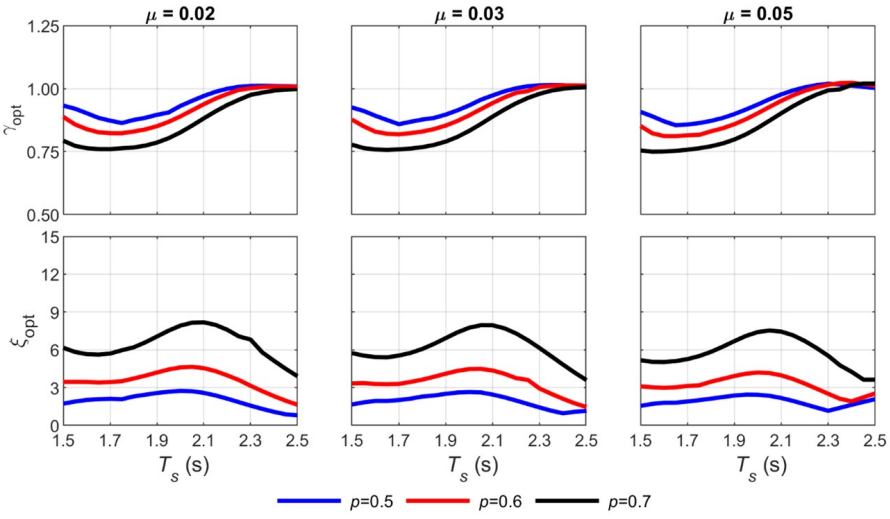

Figure 10 Optimum tuning ratio (γ_{opt}) and head loss coefficient (ξ_{opt}) as functions of the period of the primary structure (T_s), with a system damping $\xi_s = 0.05$, for a NBP.

5.2 Analysis of the TLCD efficiency

The influence of the frequency content of the excitation can be addressed through the efficiency of the optimum TLCD to reduce the displacements and accelerations of the structure, quantified using R_d and R_a respectively. These factors are defined in Eq. 31 and Eq. 32.

$$R_d = \left(1 - \frac{\sigma_{X_{W\_TLCD}}}{\sigma_{X_{W/O\_TLCD}}}\right)100 \tag{31}$$

$$R_{\mathrm{a}} = \left(1 - \frac{\sigma_{\ddot{X}_{W\_TLCD}}}{\sigma_{\ddot{X}_{W/O\_TLCD}}}\right)100 \tag{32}$$

Where $\sigma_{X_{W\_TLCD}}$ stands for the standard deviation of the main structure displacement, when the TLCD is attached to the main structure, while $\sigma_{X_{W/O\_TLCD}}$ defines the standard deviation of the main structure displacement without TLCD. Likewise, $\sigma_{\ddot{X}_{W\_TLCD}}$ is the standard deviation of the accelerations of the main structure with the TLCD, and $\sigma_{\ddot{X}_{W/O\_TLCD}}$ is the standard deviation of the acceleration of the main structure without TLCD.

5.2.1 Influence of the mass ratio in the efficiency of the TLCD

Figure 11 shows the TLCD displacement reduction efficiency with respect to the mass ratio for three values of the structure period and three length ratios. Figures 11 a) and 11 b) correspond to BBP and NBP cases, respectively. Independent of the excitation frequency, the TLCD efficiency increases as the mass ratio increases, being higher for longer length ratio values. Furthermore, for the NBP case, it can be noticed that the TLCD efficiency is even higher for structures with periods similar to the predominant period T_p of the excitation (Table 3).

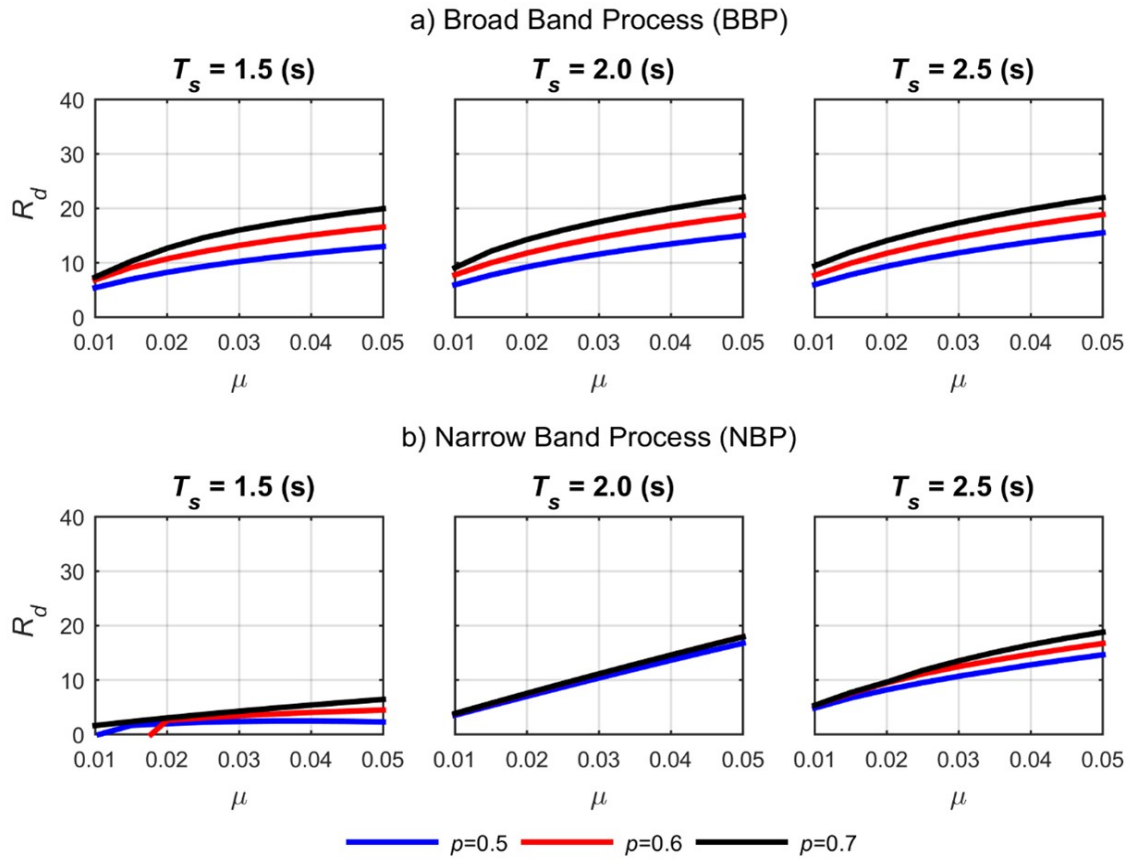

Figure 11 Displacement reduction (R_d) as a function of mass ratio (μ) with a system damping $\xi_s = 0.05$. a) Broad Band Process for and b) Narrow Band Process.

Table 3 Optimum parameters and reduction $T_s = T_p = 1.982\ (s)$ NBP.

p	0.5			0.6			0.7		
μ	0.02	0.03	0.05	0.02	0.03	0.05	0.02	0.03	0.05
ω_{opt}/ω_s	0.9240	0.9261	0.9279	0.8821	0.8856	0.8936	0.8173	0.8232	0.8346
ξ_{opt}	2.7328	2.6411	2.4243	4.5455	4.4317	4.1757	7.7898	7.6373	7.3188
T_{eq}	2.1543	2.1571	2.1789	2.2551	2.2478	2.2418	2.4274	2.4120	2.3852
R_d	9.3840	13.3746	20.2433	9.9398	14.0964	21.6759	9.6916	14.0500	21.5833
R_a	9.9690	12.9400	19.8600	9.2570	13.3900	20.7700	8.9980	13.0100	20.3500

The efficiency of the TLCD in terms of the acceleration reduction with respect to the mass ratio is presented in Figure 12. It is observed that the efficiency to control the accelerations is lower than the effectiveness achieved for the displacements for both stochastic processes (Figure 11). For the BBP case, the acceleration reduction increases with the mass ratio, but it decreases as the structure becomes more flexible. On the other hand, for the NBP motion, the same behavior of the reduction of the displacement is observed for the accelerations but with lower effectiveness for structures with $T_s = 2.5(s)$. In particular for NBP and structures with $T_s = 1.5(s)$ and $T_s = 2.0(s)$ the effect of the length ratio is not significant and R_a values are slightly larger than R_d.

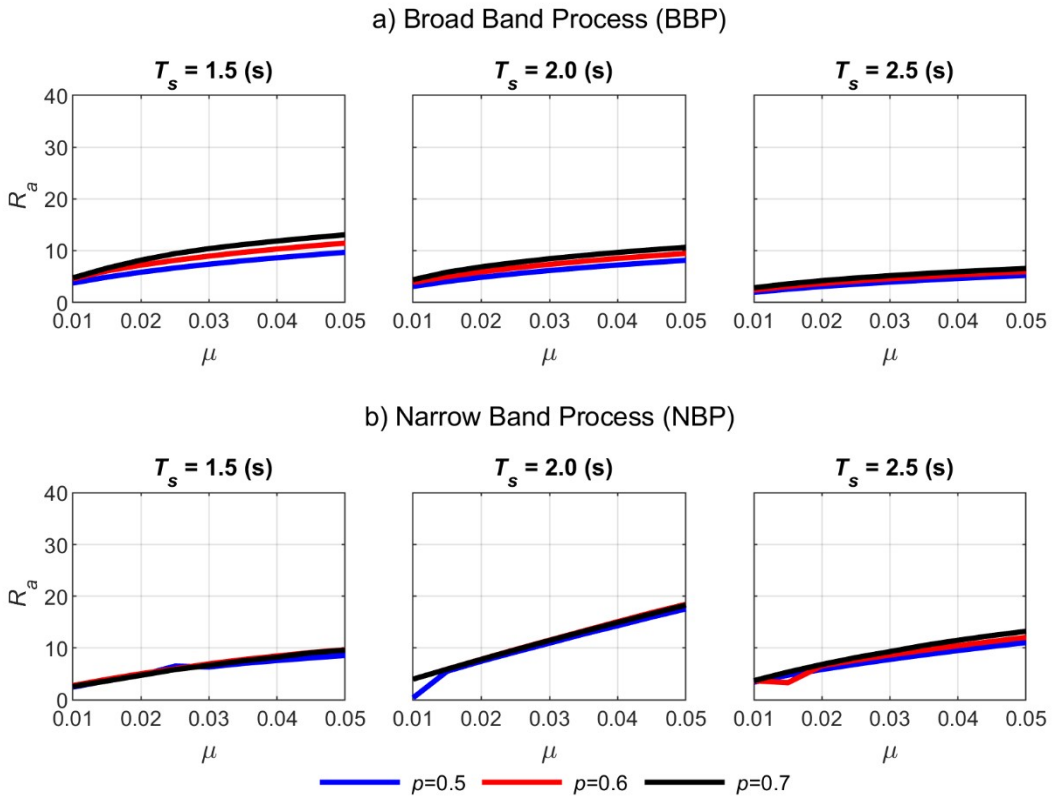

Figure 12 Acceleration reduction (R_a) as a function of mass ratio (μ) with a system damping $\xi_s = 0.05$. a) Broad Band Process for and b) Narrow Band Process.

5.2.2 Influence of the length ratio in the efficiency of the TLCD

Figure 13 shows the TLCD efficiency in reducing the displacements R_d with respect to its length ratio for three periods of the main structure and three length ratios. Figure 13 a) and Figure 13 b) correspond to BBP and NBP cases, accordingly. As shown in those figures, the TLCD is more efficient when its length ratio increases, independently of the frequency content. However, for the NBP case, the TLCD efficiency is even better for T_{eq} values close to the predominant period of the excitation.

Figures 14 a) and 14 b) present the influence of the length ratio in the reduction of the main structure's acceleration for the BBP and NBP seismic demands, respectively. It is shown that when the seismic excitation is broad-band (BBP), the

TLCD is less effective in the reduction of accelerations than displacements. However, the global behavior of the curves is analogous due to the reduction factors increment with respect to the length ratio. Besides, for the narrow-band motion (NBP), higher efficiency is obtained for the accelerations than displacements for rigid structures. Additionally, the effect of the mass ratio is also less significant in the reduction of accelerations for the BBP case and NBP with $T_s = 2.5(s)$ with regard to R_d.

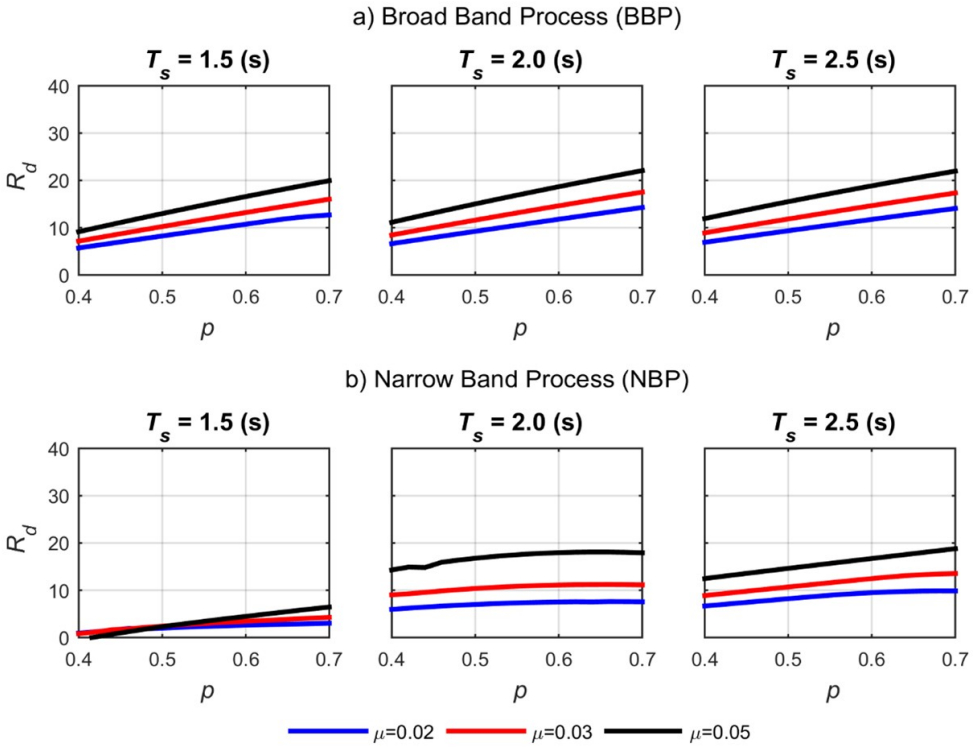

Figure 13 Displacement reduction (R_d) as a function of length ratio (p) with a system damping $\xi_s = 0.05$. a) Broad Band Process for and b) Narrow Band Process.

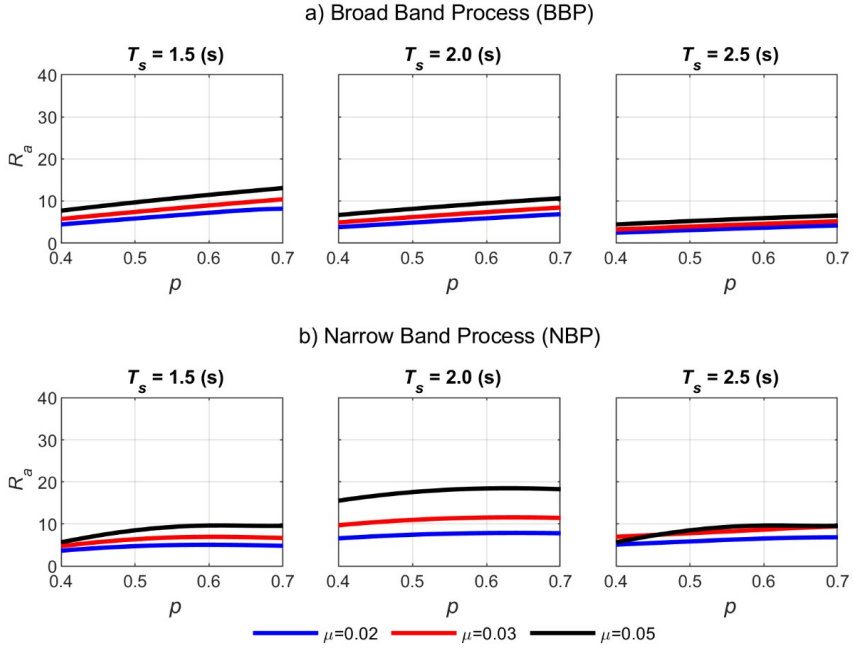

Figure 14 Acceleration reduction (R_{a}) as a function of length ratio (p) with a system damping $\xi_s = 0.05$. a) Broad Band Process for and b) Narrow Band Process.

5.2.3 Influence of the damping of the main system in the efficiency of the TLCD

Figure 15 shows the TLCD displacement reduction efficiency as a function of the main structure's damping ratio for three structure period values and three length ratio values. Similar to previous figures, Figure 15 a) corresponds to the BBP case, while Figure 15 b) represents the NBP case. TLCD efficiency decreases as the main structure damping increases. This effect is observed independently of the excitation frequency content. In the BBP case, the reduction of the optimum TLCD depends on the length ratio, being higher for longer length ratios. In contrast, for the NBP case, the TLCD efficiency is insensitive to the length ratio.

Concerning the influence of the damping of the main structure in the acceleration reduction factor, as presented in Figure 16, the decreasing behavior with respect to ξ_s is equivalent to the one observed for R_d. However, once again, the effectiveness in controlling the accelerations is lower than the reduction of displacements for the BBP process and the most flexible structure in the NBP case.

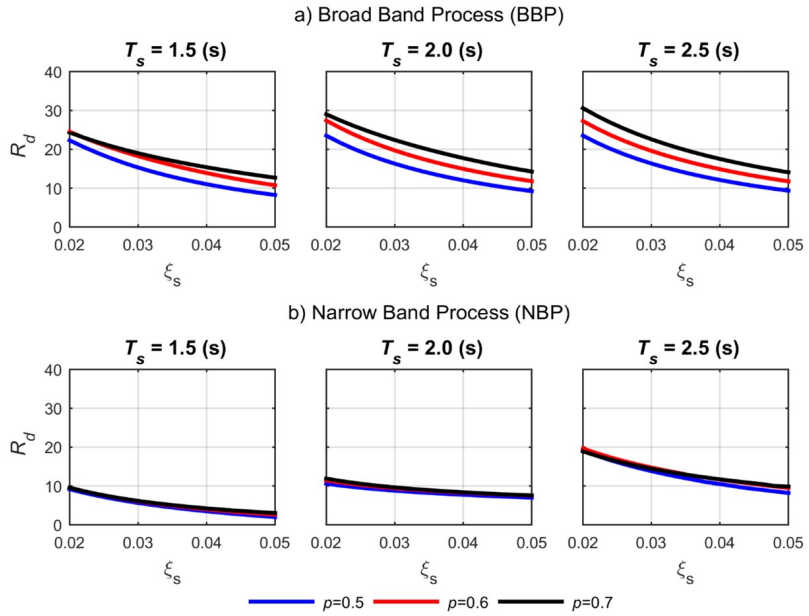

Figure 15 Displacement reduction (R_d) as a function of the main system damping (ξ_s) with a mass ratio $\mu = 0.02$. a) Broad Band Process for and b) Narrow Band Process.

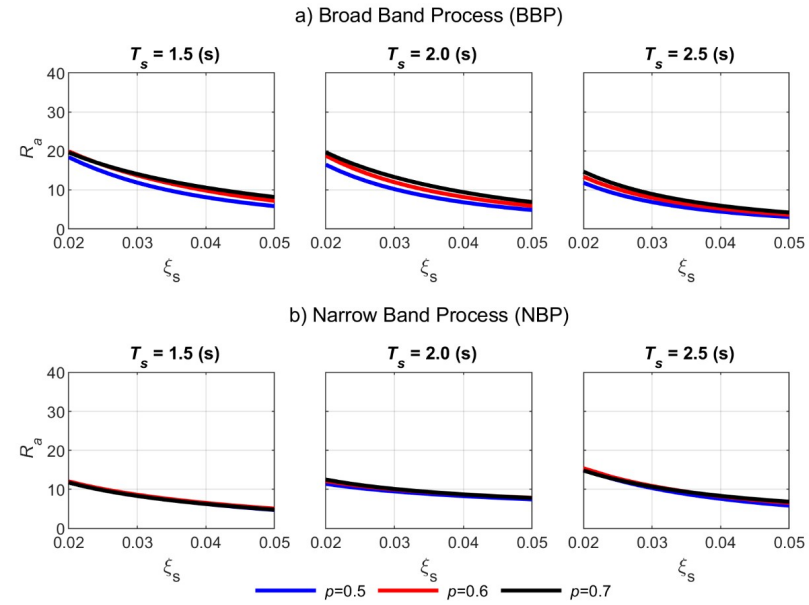

Figure 16 Acceleration reduction (R_a) as a function of the main system damping (ξ_s) with a mass ratio $\mu = 0.02$. a) Broad Band Process for and b) Narrow Band Process.

5.2.4 Influence of the main structure – TLCD equivalent period in the efficiency of the TLCD

Figure 17 shows the TLCD displacement reduction efficiency in terms of the equivalent period of the structure – TLCD system (T_{eq}) for three mass ratios and three length ratios. Figure 17 a) stands for the BBP case, and Figure 17 b) corresponds to the NBP case. As it may be noticed in Figure 17 a), the TLCD displacement efficiency is a function of the excitation bandwidth, being more efficient when excitation frequency bandwidth is broader. In general, the behavior of the displacement reduction differs in both excitations due to the existence in the NBP case of a maximum R_d value, which occurs at a T_{eq} associated with the coincidence of T_s with the predominant period of the seismic demand T_p (Table 3).

Figures 18 a) and 18 b) show the reduction factor R_{a} as a function of T_{eq}. It is observed that in high-frequency content excitations, the TLCD is less efficient in reducing accelerations than displacements. Another relevant aspect is the slope difference between R_{a} and R_d curves regarding T_{eq}. For the displacement reduction curves, it is observer a trend to increase R_d as T_{eq} becomes more flexible, while for the acceleration reduction curves, the behavior is the opposite. On the other hand, when the excitation is NBP, the efficiencies of the TLCD in the control of displacements and accelerations are very similar in shape and magnitude. Moreover, the acceleration reduction factors are less sensitive to the length ratio than the displacement reduction ratio.

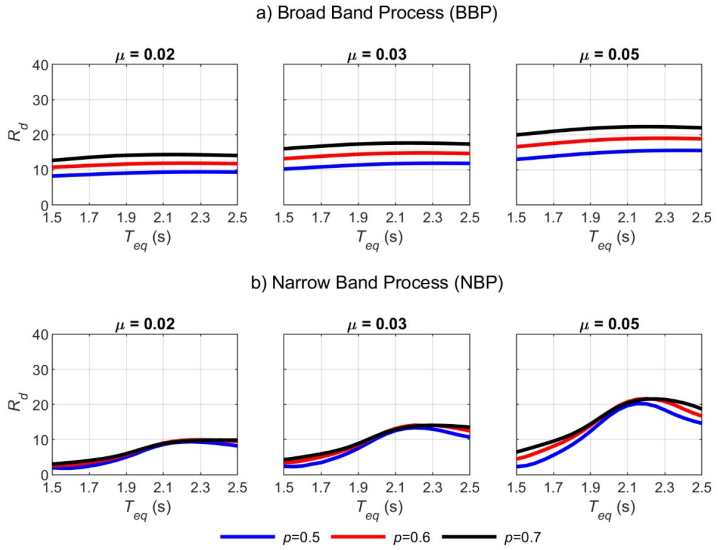

Figure 17 Displacement reduction (R_d) as a function of the equivalent structure – TLCD period (T_{eq}) with a system damping $\xi_s = 0.05$. a) Broad Band Process for and b) Narrow Band Process.

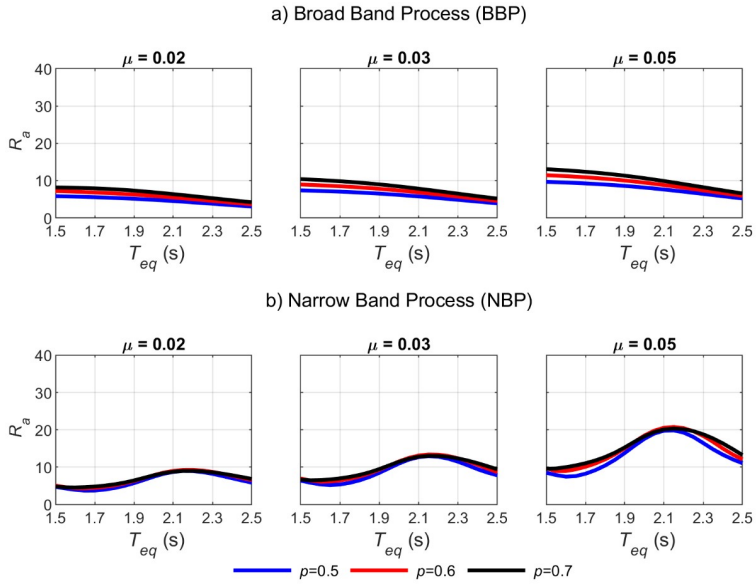

Figure 18 Acceleration reduction (R_{a}) as a function of the equivalent structure – TLCD period (T_{eq}) with a system damping $\xi_s = 0.05$. a) Broad Band Process for and b) Narrow Band Process.

5.3 Deterministic analysis of the response in time with an optimum TLCD

A deterministic analysis is performed in the following sections, considering the stochastic analysis results for both frequency contents.

5.3.1 High-frequency content excitation time-history analysis

Figure 19 shows the displacement response when the model is excited by an artificial earthquake compatible with the B soil class spectrum of the Chilean NCh2745:2013 code. In both time series plots, the main structure response addresses both the main structure response without TLCD and the main structure response when an optimum TLCD is used to control the structure.

The optimal parameters of the TLCD are presented in Table 4. A mass ratio value $\mu = 0.02$ has been considered for the main structure response showed in Figure 19 a), and in Figure 19 b) is shown the main structure response for a $\mu = 0.05$. By comparing the figures, a better TLCD efficiency in terms of displacement and acceleration is noticed when the mass ratio is higher. Besides, the reduction of the displacements is larger than the reduction of accelerations if the optimal TLCD is considered. These observations coincide with the previous stochastic analysis performed.

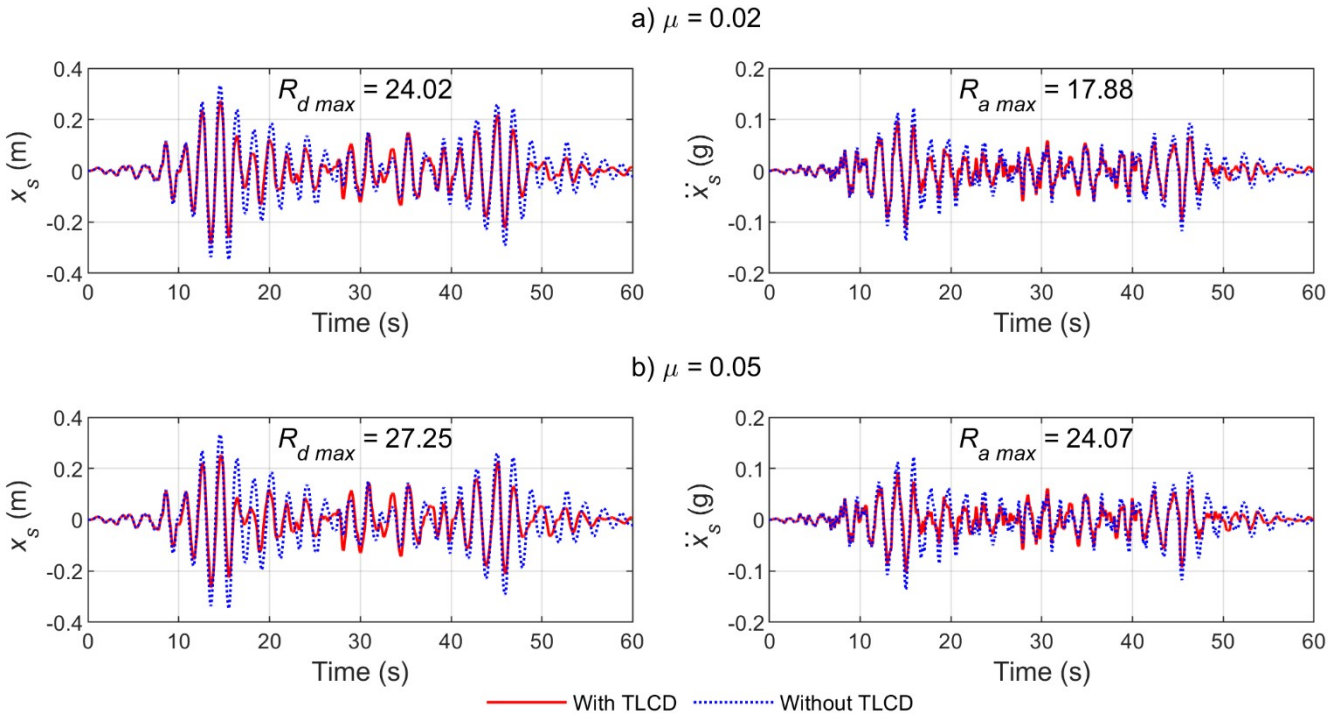

Figure 19 Main structure displacement (left) and acceleration (right) time-history when subjected to an artificial earthquake compatible with the Chilean NCh 2745 B soil class spectrum. Length ratio $p = 0.5$, $\xi = 0.05$, $T_s = 2.0\ s$. a) Mass ratio $\mu = 0.02$. b) Mass ratio $\mu = 0.05$.

Table 4 Optimal parameter of the TLCD for deterministic time-history analysis.

Seismic Input	μ	p	T_s	T_{eq}	ω_{opt}/ω_s	ξ_{opt}	R_d	R_a
BBP	0.02	0.5	2.0	2.1338	0.9753	1.7133	24.02	17.88
	0.05	0.5	2.0	2.1771	0.9601	3.0149	27.15	24.07
NBP	0.02	0.5	1.8	2.0671	0.8755	2.2962	19.11	20.06
	0.02	0.7	1.8	2.3566	0.7661	6.1922	16.78	21.79

5.3.2 Low-frequency content excitation time-history analysis

Similarly, in Figure 20 it is shown the displacement time-history response of the main structure when the model is subjected to the 1985 Mexico earthquake, which has a predominant period $T_p = 1.93\ (s)$. Figure 20 shows the main structure displacement and accelerations for a mass ratio value equals 0.02, and a damping ratio equals 0.05. The optimal parameter of the TLCD considered are showed in Table 4.

In Figure 20 a), with the considered structure period and a length ratio of $p = 0.5$, an equivalent linear period of the structure plus the TLCD of $T_{eq} = 2.078$ (s) is obtained, which coincides, approximately, with the predominant period of the excitation T_p. In Figure 20 b), the main structure period T_s is again 1.8 (s) but, in contrast with Figure 20 a), the length ratio is $p = 0.7$, giving an equivalent linear period $T_{eq} = 2.356$ (s), far away from the predominant excitation period.

As shown in Figure 20, there is a reduction in the maximum main structure displacement and acceleration when the TLCD is attached. In this case, the reduction of accelerations is larger than the reduction of displacements for both $p = 0.5$ and $p = 0.7$. Although there are differences in magnitude, this result follows the findings of the stochastic analysis presented in Figure 13 and Figure 14, where is showed that for a mass ratio $\mu = 0.02$ the values of R_{a} are larger than R_d for the NBP process in the whole studied range of the length ratio.

Concerning the displacemt reduction, the R_d obtained in Figure 20 a) is higher than the one obtained when the TLCD is employed with the system parameters specified in Figure 20 b). This fact also verifies the result derived from the stochastic analysis (i.e., Figure 17 b), where it is concluded that the highest displacement reduction for the NBP case occurs when the structure has a period that causes a tuning between the excitation predominant period and main system-TLCD linear equivalent period.

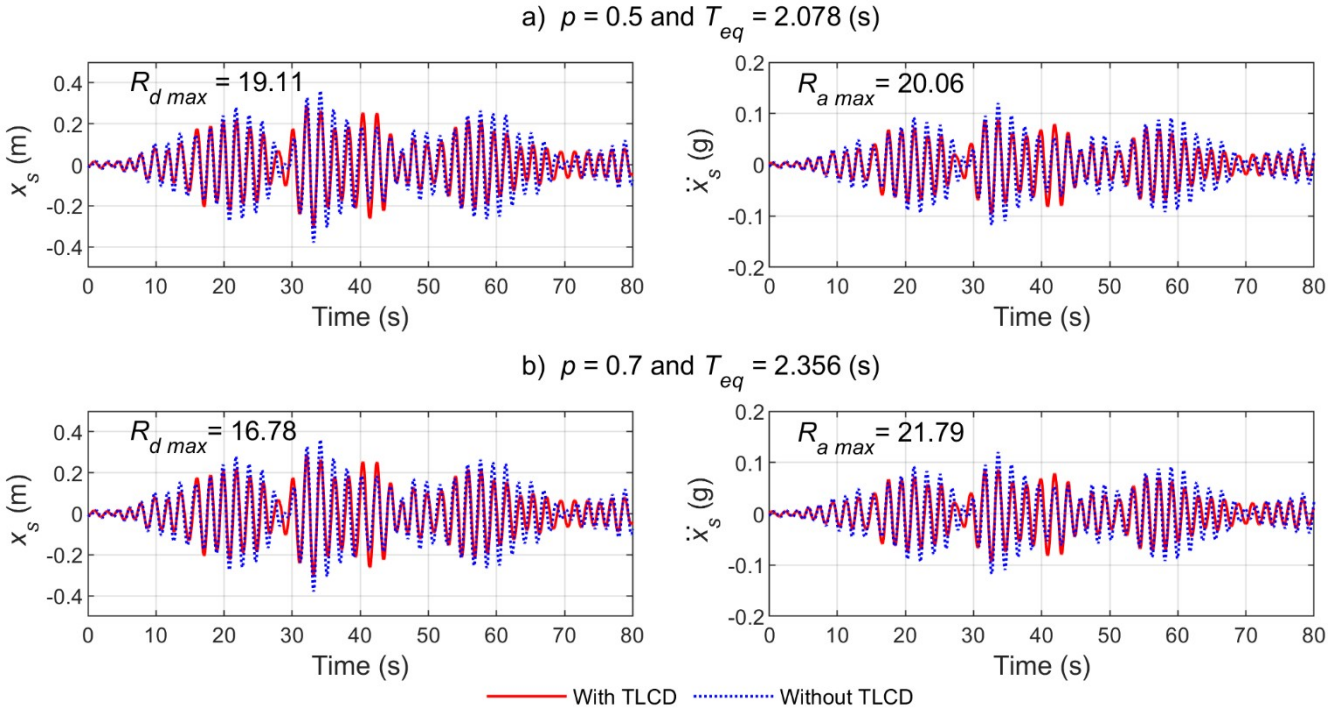

Figure 20 Main structure *displacement (left) and acceleration (right)* time-history when subjected to the 1985 Mexico Earthquake. Mass ratio $\mu = 0.02$, $\xi = 0.05$, $T_s = 1.8\ s$. a) Length ratio $p = 0.5$ and $T_{eq} = 2.078\ (s)$. b) Length ratio $p = 0.7$ and $T_{eq} = 2.356\ (s)$.

6 CONCLUSION

Form the results obtained in this study; it may be concluded the following:

1. The TLCD efficiency depends on the frequency bandwidth of the seismic excitation, being more effective for excitations with high-frequency content.
2. When subjected to a broad frequency bandwidth excitation:
   a. The optimum frequency of the TLCD tends to be perfectly tuned to the main system frequency, being practically insensitive to the variation of the TLCD and main structure parameters addressed in the current investigation.
   b. The optimum TLCD head loss coefficient has higher values as its mass ratio and length ratio increase, and when the structure is more flexible.

c. The TLCD is more efficient when the mass ratio, length ratio, and main structure period are higher. In contrast, it is less efficient as the main structure damping increases.

3. When subjected to a narrow frequency bandwidth excitation:
   a. The TLCD optimum properties are very sensitive to the parameters considered in the study.
   b. The optimum tuning ratio behaves differently in very flexible structures ($T_s > 2\ (s)$), approaching to be perfectly tuned to the main structure. The optimum value does not depend on the mass ratio of the TLCD, nor of the main structure damping coefficient.
   c. If $T_s < 2.5\ (s)$ the optimum tuning ratio depends slightly on the mass ratio and the damping ratio, being lower if the damping ratio is smaller. However, the optimum tuning ratio is very sensitive to the TLCD length ratio, being higher if this ratio is increased. It is also sensitive to the main structure period, reaching a minimum for the period that matches the system's equivalent linear period with the TLCD device attached. This equivalent linear period coincides with the predominant period of seismic excitation.
   d. The TLCD head loss coefficient behaves differently in very flexible structures (T_s> 2 s), keeping the same behavior in more flexible structures, but with a lower value. As the main system turns out rigid, a significant sensitivity occurs with respect to the length ratio, decreasing its value with respect to the length ratio. Sensitivity is also noticeable regarding the structure period, reaching a maximum value that corresponds to the structure period value in which an inflection point at the frequency ratio curves occurs.
   e. The TLCD performance is better for larger mass and length ratios and tends to be less efficient as the structure's damping ratio increases. The maximum TLCD performance occurs when the main structure period coincides with the predominant seismic excitation period. In this case, the optimum TLCD frequency tunes the linear equivalent period of the system TLCD-structure.
   f. Although the NBP case was considered to have a long predominant period in this study, results suggest that the findings could be extended to narrow-banded seismic demands independently of the value of its predominant period. Further research is needed.
4. In general terms, the effectiveness of the TLCD to reduce the accelerations is lower than efficiency to reduce the displacements. However, in certain cases when the structural period is short ($T_s < 2.0\ s$), the mass ratio of the TLCD is small, and the seismic demand possesses a narrow content of frequencies, the capability of the TLCD to reduce the accelerations is larger than the reduction of displacements.
5. The results of the deterministic analysis verify the results of the research conducted in the stochastic context.

Acknowledgements

The authors would like to thank the support provided by Prof. José Luis Almazán of the Pontifical Catholic University of Chile. His collaboration with the numerical analyses is sincerely acknowledged. The authors gratefully acknowledge the University of Bio-Bio Research Direction for funding this research under grant DIUBB 2060542 IF/R.

Author's Contribuitions: Conceptualization, G Espinoza; Methodology, G Espinoza; Investigation, C Romero, G Espinoza, F Benedetti; Writing - original draft, G Espinoza and F Benedetti; Writing - review & editing, F Benedetti and G Espinoza; Visualization, F Benedetti; Supervision, G Espinoza; Software, G Espinoza.

Editor: Jan Awrejcewicz.

References

Almazán, J., Espinoza, G., Aguirre, J. (2012). Torsional balance of asymmetric structures by means of tuned mass dampers. Engineering Structures 42:308-328.

Altunişik, A.C., Yetişken, A., Kahya, V. (2017). Experimental study on control performance of tuned liquid column dampers considering different excitation directions. Journal of Mechanical Systems And Signal Processing 102:59-71.

Chakraborty, S., Debbarma, R., Marano, G.C. (2011). Performance of tuned liquid column dampers considering maximum liquid motion in seismic vibration control of structures. Journal of Sound And Vibration 331(7):1519-1531.

Chakraborty, S., Debbarma, R., Marano, G.C. (2012). Performance of tuned liquid column dampers considering maximum liquid motion in seismic vibration control of structures. Journal of Sound and Vibration 331(7):1519-1531.

Clough, R.W. and Penzien, J. (1975). Dynamics of structures. Mc Graw-Hill (New York).

Den Hartog, J. (1956). Mechanical Vibrations, McGraw-Hill (New York).

INN. (2013). National Normalization Institute. NCh2745:2013 Analysis and design of buildings with seismic isolation (in Spanish: Análisis y diseño de edificios con aislación sísmica). Chile.

Iwan, W.D. and Yang, I.M. (1972). Application of statistical linearization techniques on nonlinear multi-degree of freedom systems. Journal of Applied Mechanics 39(2):545-550.

Kavand, A. and Zahrai, S.M. (2006a). Impact of the seismic excitation characteristics on the efficiency of tuned liquid column dampers. Earthquake Engineering and Engineering Vibration 5(2):235-243.

Kavand, A. and Zahrai, S.M. (2006b). An investigation on the effects of earthquake excitation parameters on the effectiveness of Tuned Liquid Column Dampers. In Proceedings of the 5th Internation Conference on Beahaviour of Steel Structures in Seismic Areas. STESSA 2006. CRC Press.

Lee, S.K., Lee, H.R., Min, K.W. (2010). Experimental verification on nonlinear dynamic characteristic of a tuned liquid column damper subjected. The Structural Design of Tall and Special Buildings 21:374–388.

Lin, Y.Y., Cheng, C.M., Lee, C.H. (2000). A tuned mass damper for suppressing the coupled flexural and torsional buffeting response of long-span bridges. Engineering Structures 22(9):1195-1204.

Mayoral, J.M., Asimaki, D., Tepalcapa, S., Wood, C., Roman-de la Sancha, A., Hutchinson, T., Franke, K., Montalva, G. (2019). Site effects in Mexico City Basin: Past and present. Soil Dynamics and Earthquake Engineering 121:369-382.

Park, B., Lee, Y., Park, M., Ju, Y.K. (2018). Vibration control of a structure by a tuned liquid column damper with embossments. Engineering Structures 168:290-299.

Rozas, L., Boroschek, R.L., Tamburrino, A., Rojas, M. (2015). A bidirectional tuned liquid column damper for reducing the seismic response of buildings. Structural Control and Health Monitoring 23:621–640.

Sadek, F., Mohraz, B., Taylor, A.W., Chung, R.M. (1997). A method of estimating the parameters of tuned mass dampers for seismic applications. Earthquake Engineering & Structural Dynamics 26(6):617-635.

Saitua, F., Lopez-Garcia, D., Taflanidis, A.A. (2018). Optimization of height-wise damper distributions considering practical design issues. Engineering Structures 173:768-786.

Sakai, F., Takeda, S., Tamaki, T. (1989). Tuned liquid column damper-new type device for suppression of building vibration. Proceedings of the International Conference on High-Rise Buildings, Nanjing, China 926-931.

Shum, K.M. (2009). Closed form optimum solution of a tuned liquid column damper for suppressing harmonic vibration of structures. Engineering Structures 31(1):84-92.

Ueng, J.M., Lin, C.C., Wang, J.F. (2008). Practical design issues of tuned mass dampers for torsionally coupled buildings under earthquake loading. Structural Design of Tall and Special Building 17(1):133-165.

Wu, J.C., Shih, M.H., Lin, Y.Y. (2005). Design guidelines for tuned liquid column damper for structures responding to wind. Engineering Structures 27(13):1893-1905.

Xu, Y.L., Samali, B., Kwok, K.C.S. (1992). Control of along-wind response of structures by mass and liquid dampers. Journal of Engineering Mechanics 118(1):20-39.

Xu, Y.L. and Shum, K.M. (2003). Multiple-tuned liquid column dampers for torsional vibration control of structures: theoretical investigation. Earthquake Engineering and Structural Dynamics 32(2):309–328.

Zahrai, S.M. and Kavand, A. (2008). Strong ground motion effects on seismic response reduction by TLCDs. Scientia Iranica 15(3):275-285.